Materials Today Bio 28 (2024) 101175

Contents lists available at ScienceDirect

Materials Today Bio

journal homepage: www.journals.elsevier.com/materials-today-bio

Melatonin-loaded bioactive microspheres accelerate aged bone regeneration by formation of tunneling nanotubes to enhance mitochondrial transfer

Huacui Xiong [a,d], Huanhuan Qiu [d], Chunhui Wang [d], Yonghao Qiu [d], Shuyi Tan [d], Ke Chen [d,**], Fujian Zhao [d,***], Jinlin Song [a,b,c,*]

[a] Stomatological Hospital of Chongqing Medical University, Chongqing, 401147, China
[b] Chongqing Key Laboratory of Oral Diseases and Biomedical Sciences, Chongqing, 401147, China
[c] Chongqing Municipal Key Laboratory of Oral Biomedical Engineering of Higher Education, Chongqing, 401147, China
[d] Stomatological Hospital, School of Stomatology, Southern Medical University, Guangzhou, 510280, China

ARTICLE INFO

Keywords:
Mesoporous bioactive glasses
Aged bone regeneration
Mitochondrial function
Mitochondrial transfer
Tunneling nanotubes

ABSTRACT

The repair of bone defects in the elderly individuals is significantly delayed due to cellular senescence and dysfunction, which presents a challenge in clinical settings. Furthermore, there are limited effective methods available to promote bone repair in older individuals. Herein, melatonin-loaded mesoporous bioactive glasses microspheres (MTBG) were successfully prepared based on their mesoporous properties. The repair of bone defects in aged rats was significantly accelerated by enhancing mitochondrial function through the sustained release of melatonin and bioactive ions. MTBG effectively rejuvenated senescent bone marrow mesenchymal stem cells (BMSCs) by scavenging excessive reactive oxygen species (ROS), stabilizing the mitochondrial membrane potential (ΔΨm), and increasing ATP synthesis. Analysis of the underlying mechanism revealed that the formation of tunneling nanotubes (TNTs) facilitated the intercellular transfer of mitochondria, thereby resulting in the recovery of mitochondrial function. This study provides critical insights into the design of new biomaterials for the elderly individuals and the biological mechanism involved in aged bone regeneration.

1. Introduction

As life expectancy has increased, the issue of population aging has become more prominent. Bone defects are common among elderly individuals due to bone loss and weakened bone strength [1]. As a result of organ deterioration, the repair of bone defects is significantly delayed, which greatly affects quality of life [2,3]. To date, only a limited number of studies have documented the application of bioactive materials for bone repair in aged scenarios [4,5]. However, these materials have shown limited efficacy in delaying cellular senescence or rejuvenating senescent cells, resulting in suboptimal bone regeneration outcomes. Consequently, the clinical challenge of repairing bone defects remains unresolved among the elderly population. Therefore, there is an urgent clinical necessity to develop bone repair materials specifically tailored to this demographic.

Bioactive glasses (BG), especially mesoporous bioactive glasses with the property of excellent cytocompatibility and rapid ion dissolution, are known for their superior osteoconductive and osteoinductive properties, thus, they are widely used to treat bone defects [6,7]. Additionally, mesoporous BG exhibits a highly ordered mesoporous structure ranging from 2 to 50 nm and possesses a significantly high specific surface area and pore volume, enabling precise control over the loading and release processes of biomolecules and drugs [8]. In mesoporous BG, biomolecules and drugs can be loaded in the mesoporous channel through soaking techniques or surface grafting and can then be released in a sustained manner [9]. All these characteristics contribute to the suitability of mesoporous BG as an effective drug delivery system [9]. Although mesoporous BG is unable to delay cellular senescence or enhance the function of senescent cells, it presents a distinctive advantage for loading anti-aging agents.

* Corresponding author. Stomatological Hospital of Chongqing Medical University, Chongqing, 401147, China.
** Corresponding author.
*** Corresponding author.
E-mail addresses: dentchenke@163.com (K. Chen), zhaofj@smu.edu.cn (F. Zhao), songjinlin@hospital.cqmu.edu.cn (J. Song).

https://doi.org/10.1016/j.mtbio.2024.101175
Received 15 March 2024; Received in revised form 3 June 2024; Accepted 29 July 2024
Available online 2 August 2024

The indole hormone melatonin (N-acetyl-5-methoxytryptamine) is primarily secreted by the pineal gland [10]. It has various functions, including scavenging free radicals [11], promoting and regulating energy homeostasis [12,13] and delaying senescence [14]. Melatonin has also been shown to stimulate the commitment and differentiation of bone marrow mesenchymal stem cells (BMSCs) into osteoblasts [15,16]. However, oral administration of melatonin results in a relatively limited concentration reaching the bone defect, leading to suboptimal bone regeneration. To date, studies in the literature documenting the application of bioactive microspheres incorporating melatonin in aged bone regeneration are lacking. Hence, in this study, we synthesized melatonin-loaded bioactive glasses microspheres (MTBG) and investigated their potential to enhance bone tissue regeneration in aged rats.

Mitochondria manage cellular energy production and are intricately involved in various biological processes, including cellular metabolism [17,18], growth [19], differentiation [20] and aging [21,22]. A decline in mitochondrial function occurs with aging [23,24]. Senescent cells exhibit increased leakage of mitochondrial proteins, a reduced mitochondrial membrane potential (ΔΨm), and an excessive accumulation of reactive oxygen species (ROS) in mitochondria, resulting in decreased energy supply [25,26]. Due to the decreased mitochondrial function in senescent BMSCs, their proliferation and differentiation abilities are significantly compromised [27]. Therefore, improving mitochondrial function is an effective method for promoting the osteogenesis of senescent BMSCs, thus leading to the promotion of bone regeneration in elderly individuals.

Mitochondrial transfer refers to the translocation of mitochondria from one cell to other cells via specialized structures under both physiological and pathological circumstances [28,29]. This transfer process has been proven to be an effective method for restoring mitochondria in injured cells [30]. Tunneling nanotubes (TNTs) are considered the major structure involved in mitochondrial transfer [31]. It remains unclear whether MTBG can accelerate age-related osteogenesis via mitochondrial transfer through TNT formation. In this study, we established an *in vitro* senescence model of BMSCs, thoroughly examined the impact of MTBG on mitochondrial function, and conducted comprehensive investigations into its underlying mechanisms (Fig. 1).

2. Materials and methods

2.1. Synthesis and characterization of MTBG

The preparation of mesoporous bioactive glasses microspheres was conducted in accordance with our previously published study [32].The detailed procedures for the preparation of mesoporous BG are provided in the supplementary data. MTBG was prepared through mesoporous adsorption. In brief, melatonin (Aladdin Chemical, Shanghai, China) was dissolved in anhydrous ethanol at a concentration of 45 mg/L. After 100 mg of BG was dispersed, the solution was stirred at 37 °C at 200 rpm for 24 h. The solution was then subjected to centrifugation at 10000×*g* for 5 min at 4 °C. Afterward, the supernatant was collected and quantified using UV–Vis spectroscopy (Miulab, China) at a wavelength of 279 nm. Finally, the samples were air-dried to obtain the MTBG.

The morphological features, phase composition and chemical composition of the MTBG and mesoporous BG were analyzed using advanced techniques, including scanning electron microscopy (FE-SEM, Zeiss Sigma 300, Germany), X-ray diffraction (XRD, Rigaku ULTIMA IV, Japan) and Fourier transform infrared spectroscopy (FTIR, Bruker TENSOR 27, Germany). Transmission electron microscopy (TEM, FEI Tecnai G2 F20 S-Twin, USA) was used to visualize the microstructure of

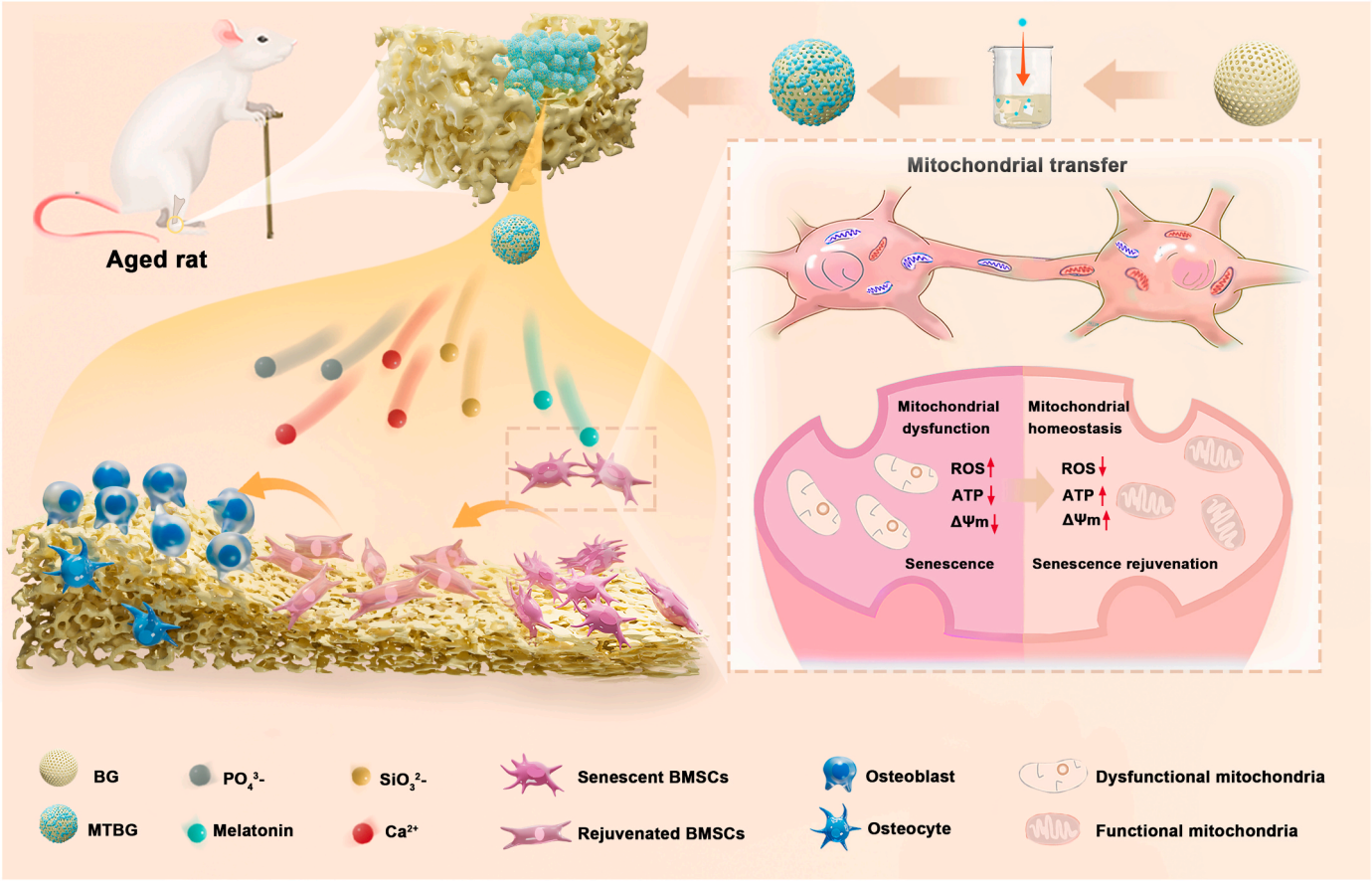

Fig. 1. Schematic illustration of the proposed mechanism for accelerating aged bone regeneration via enhancing mitochondrial transfer mediated by tunneling nanotubes using melatonin-loaded bioactive microspheres (MTBG).

the particles, and energy-dispersive X-ray spectroscopy (EDS) was used to measure the elemental content. Selected area electron diffraction (SAED) patterns were taken in the TEM mode. The zeta potential was detected by a Malvern Zetasizer Nano As (Malvern, UK). The multipoint Brunauer–Emmett–Teller (BET) N_2 absorption technique at 77.3 K was employed for the determination of the specific surface area, while the Barrett–Joyner–Halenda (BJH) method was utilized to derive pore size and distribution from the isotherm. Thermogravimetric analysis (TGA) was performed using a TGA/DSC3+ thermal analysis system (Mettler Toledo, Switzerland).

The melatonin release of the MTBG was assessed by dispersing 10 mg of MTBG in 3 mL of normal saline and subjecting it to agitation at a speed of 100 rpm at 37 °C. The sample was immersed for a predetermined duration and subsequently centrifuged. The supernatant was sampled by withdrawing 1 mL and simultaneously replenishing it with 1 mL of fresh saline solution. The supernatant was subjected to UV–Vis spectroscopy (Miulab, China) at a wavelength of 279 nm to measure its absorbance, enabling the calculation of melatonin concentration and determination of the quantity released at a specific time. A standard curve of melatonin was established by measuring the absorbance at 279 nm across various concentrations of melatonin solution, yielding a highly significant correlation coefficient ($R^2 = 0.9955$) (Fig. S1). The encapsulation efficiency (%) was calculated by dividing the weight of melatonin that was encapsulated by the initial weight of melatonin. The drug loading efficiency (%) was calculated by dividing the weight of melatonin that was encapsulated by the weight of mesoporous BG.

To assess the release of ions from BG and MTBG microspheres, 100 mg of microspheres were immersed in 5 mL of simulated body fluid (SBF) with a pH of 7.4 at 37 °C for 1, 4, and 7 days. The concentrations of calcium (Ca), silicon (Si), and phosphorus (P) ions in the SBF were quantified using an inductively coupled plasma mass spectrometer (ICP-MS, Agilent, USA) at each time point.

2.2. Evaluation of cellular senescence

Tert-butyl hydroperoxide (tBHP, Macklin, China) was utilized to induce cellular senescence according to a previous study [33]. Mouse BMSCs (Cyagen Biosciences, China) at passages 3 to 8 were used for subsequent investigations. To demonstrate the effect of MTBG and BG on BMSCs through ion dissolution and melatonin release, MTBG and BG extracts were used in *in vitro* experiments. Initially, the cells were treated with tBHP for 2 h after which the medium was replaced with normal growth medium, melatonin, BG extracts, or MTBG extracts. Subsequently, the cells were cultured for an additional 24 h. Cells without tBHP treatment were considered the normal group. Subsequently, cell assessment was conducted using a β-galactosidase activity assay. Additionally, the protein expression levels of p16, p21 and p53 were analyzed by western blotting. For assessments of osteogenic differentiation, cells were exposed to osteogenic induction medium supplemented with different extracts. After 21 days, alizarin red staining was performed to assess the osteogenic potential of the cells. Additionally, the protein and gene expression levels of OCN were analyzed by immunofluorescence staining and qRT−PCR analysis. For immunofluorescence staining, a rabbit anti-OCN antibody (1:350, Proteintech, China) was used. Detailed information regarding the experimental approaches mentioned above, including the extract preparation procedures, can be found in the supplementary data.

2.3. Evaluation of mitochondrial function

After treatment, the cells were processed for evaluation of mitochondrial function. Mitochondrial morphology was observed using TEM. The cells were delicately scraped and subjected to centrifugation at 300×*g* for 2 min. The pellets were further fixed in 2.5 % glutaraldehyde before being prepared for TEM (HT7700, HITACHI Japan) observation. Detailed information regarding the experimental approaches can be found in the supplementary data.

The mitochondrial membrane potential and the levels of intracellular and mitochondrial ROS were assessed using a JC-1 Assay Kit (Bestbio, China), a DCFH-DA probe (Beyotime, China) and a mitoSOX probe (MedChemExpress, USA), respectively. The cells were washed and incubated with JC-1 staining working solution or complete medium containing either 10 μM DCFH-DA or 5 μM MitoSOX in the dark for 20 min at 37 °C. After washing, the cells were immediately observed using a confocal laser microscope or analyzed utilizing flow cytometry (DxFLEX, USA).

Intracellular adenosine triphosphate (ATP) production in BMSCs was quantified by utilizing an ATP assay kit (Solarbio, China) following the manufacturer's instructions. Initially, the cells were washed and lysed in ATP extraction reagent. Subsequently, the samples were sonicated for 1 min and centrifuged at a speed of 10000×*g* for 10 min. The resulting supernatant was combined with 500 μL of chloroform and maintained at a low temperature on ice before quantification. The absorbance values at 0 min (A1) and 3 min (A2) were measured at 37 °C and 340 nm using an ultramicro ultraviolet–visible spectrophotometer (Miulab, China).

2.4. Assessment of mitochondrial transfer

The cells were initially examined for the presence of TNTs. After treatment, the cells were cultivated in the dark at 37 °C with 200 nM MitoTracker Red (Beyotime, China) for 20 min. After being washed with PBS and fixed with 4 % paraformaldehyde, the cells were permeabilized using 0.1 % Triton X-100. The cells were then stained for F-actin using Phalloidin-iFluor 488 Reagent (Abcam, United Kingdom) for another 20 min. Meanwhile, the nuclei were counterstained with DAPI (Beyotime, China). A confocal laser microscope (Leica, Germany) was employed to observe the formation of TNTs. Z-stacks spanning from the bottom to the top of the cells were also acquired in order to visualize mitochondria within TNTs.

To further investigate the intercellular mitochondrial transfer, cells were labeled separately with MitoTracker Red and carboxyfluorescein diacetate succinimidyl ester (CFDA SE) probes (Warbio, China) following the manufacturer's instructions. After treatment, cells labeled with the different probes were digested with 0.25 % pancreatin and mixed at a 1:1 ratio before being seeded onto sterile coverslips in 24-well plates. The cells were then cultured with normal growth medium or MTBG extracts for an additional 24 h. To clarify the effect of TNTs on mitochondrial transfer, 200 nM cytochalasin B (CB, MedChemExpress) was added to the MTBG extracts. After washing the cells again with PBS, they were then fixed, permeabilized and stained for F-actin using Alexa Fluor 405 Phalloidin (Jiangsu Jikai Biotechnology, China). Finally, the cells were observed using confocal microscopy (Leica, Germany). Furthermore, the gene and protein expression profiles of markers associated with mitochondrial function and mitochondrial transfer were also examined. Detailed information regarding the experimental approaches is provided in the supplementary data.

2.5. In vivo bone regeneration evaluation

Male Sprague-Dawley (SD) rats aged 18 months and weighing 800–1000 g (Fig. S7) were obtained from the Laboratory Animal Center at Southern Medical University. The animal procedures were conducted in strict accordance with the approved protocol of the Institutional Animal Care and Use Committee (Guangdong Pharmaceutical University) (Reference number: gdpulacspf2022112). The rats were randomly allocated to three groups: the control, BG, and MTBG groups. The surgical procedures were conducted under general anesthesia with an intraperitoneal injection of pentobarbital (Nembutal, 3.5 mg/100 g). The femoral condyle was subjected to the creation of a cylindrical defect with a diameter and depth of 3 mm. Subsequently, the bone defects were filled with 15 mg of either BG or MTBG particles (Fig. S8). At 6 weeks

postimplantation, three rats from each group were sacrificed, and their femoral bones were promptly excised and fixed in a 4 % paraformaldehyde solution. All samples were scanned using microcomputed tomography (micro-CT, Bruker SkyScan1276, Germany) with a voltage of 85 kV and an electric current of 200 μA. Three-dimensional images were reconstructed using NRecon software (Bruker, Germany) based on the micro-CT results.

After scanning, all the samples were subjected to a 6-week decalcification process in 10 % EDTA solution, after which they were embedded in paraffin. The samples were prepared for histological analysis by sectioning and staining with hematoxylin and eosin (H&E) as well as Masson's trichrome. Additionally, the samples were subjected to immunofluorescence staining for RUNX2 (1:50, Proteintech), OCN (1:50, Proteintech), and collagen I (1:50, Proteintech) and double-stained for Miro1 (1:100, Boster Biotech, China) and PGC1α (1:200, Proteintech). Images were acquired using a fluorescence microscope (Leica, Germany), and the fluorescence intensity was quantified utilizing Image J software.

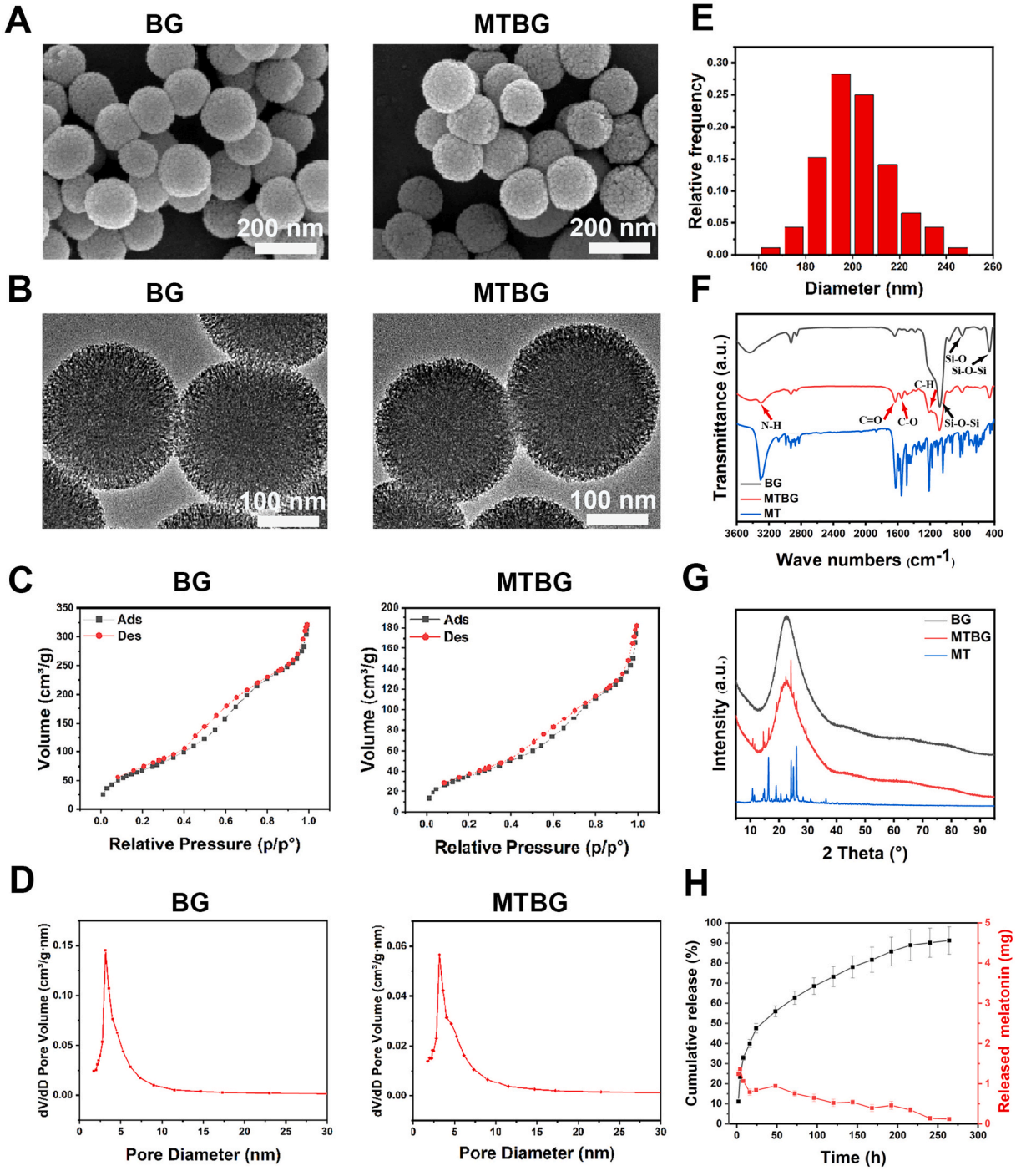

Fig. 2. Characterizations of BG and MTBG. (A) SEM images of BG and MTBG; (B) TEM images showing the mesoporous structures of BG and MTBG; (C) BG and MTBG based on N_2 adsorption—desorption analysis; (D) Pore size distributions of BG and MTBG; (E) Particle size distribution diagram of MTBG; (F) FTIR spectra showing the chemical structures of BG, melatonin and MTBG; (G) XRD patterns presenting the typical amorphous structures of BG, melatonin and MTBG; (H) Melatonin release profile of MTBG *in vitro*.

2.6. Statistical analysis

All the data are measured and presented as the mean ± standard deviation (SD). Statistical significance was determined using two-sample *t*-test or one-way analysis of variance (ANOVA) with the least significant difference (LSD) post hoc tests, and differences were considered significant at $P < 0.05$.

3. Results

3.1. Characterization and cell biocompatibility of MTBG

In this study, MTBG was successfully prepared by a mesoporous adsorption method. The SEM images revealed that both BG and MTBG exhibited regular spherical morphologies, characterized by uniform particle sizes of approximately 200 nm (Fig. 2A and E). The TEM images demonstrated the preservation of the ordered mesoporous structure even after melatonin loading (Fig. 2B), and the samples exhibited elemental compositions consistent with those of BG (Figs. S2C and D). The SAED patterns of both BG and MTBG exhibited diffuse ring patterns (Figs. S2A and B), indicating their amorphous properties, which was consistent with the XRD results (Fig. 2G). As shown in Fig. S3, the average zeta potentials of BG and MTBG were −0.55 mV and −6.05 mV, respectively. The N_2 absorption-desorption isotherm results provided additional evidence that both BG and MTBG demonstrated a characteristic type IV curve with a type H3 hysteresis loop (Fig. 2C). The pore diameter was distributed around 4 nm (Fig. 2D).

The loading efficiency and release characteristics of melatonin were further investigated. The major peaks of melatonin were detected at 3303 cm^{-1} (N–H), 1629 cm^{-1} (C=O), 1555 cm^{-1} (C–O) and 1212 cm^{-1} (C–N), indicating the successful loading of melatonin (Fig. 2F). The encapsulation and loading rates were 62.81 % and 12.56 %, respectively. The results of the TGA analysis are presented in Fig. S4. The drug loading of melatonin was calculated to be approximately 9.41 wt% by comparing the respective weight loss data. The drug release profile of MTBG is illustrated in Fig. 2H. The melatonin exhibited an initial burst release within 24 h, with the cumulative release rate reaching 47.52 ± 2.34 % at this time point, followed by a sustained release phenomenon. The cumulative release rate finally reached 91.24 ± 6.84 %. The release profiles of other elements, such as Ca, Si, and P, exhibited a similar patterns to that of melatonin, with rapid release within the first 24 h. Subsequently, the rates of release gradually slowed (Fig. S5).

The proliferation of BMSCs cultured with MTBG was determined with a CCK-8 assay (Fig. S6). The cells exhibited a rapid growth rate starting on day 3. Additionally, the proliferative capacity of the MTBG group was superior to that of the control group on day 7, indicating the beneficial impact of MTBG on cellular proliferation.

3.2. MTBG accelerates in vivo bone regeneration of in aged rats

To further investigate the potential of inducing *in situ* bone regeneration in aged rats, BG and MTBG were implanted into femoral bone defects, while rats with untreated empty femur defects were used as a control group. At 6 weeks after implantation, the rats were euthanized, and micro-CT analysis was performed to evaluate the extent of new bone formation. The blank group exhibited a limited amount of bone tissue surrounding the defect periphery, whereas the BG group demonstrated enhanced new bone formation. The MTBG group exhibited significantly greater formation of new bone (Fig. 3A). The quantitative micro-CT analysis revealed significantly greater bone volume to total volume ratio (BV/TV), bone mineral density (BMD), and trabecular number (Tb.N) in the MTBG group compared to the control and BG groups, providing further confirmation of substantial new bone formation in the MTBG group (Fig. 3B, C and Fig. S9).

Next, samples were subjected to H&E and Masson's trichrome staining to provide a more detailed analysis. In the blank group, the bone defect region remained predominantly unoccupied, with only sparsely distributed fibrous tissue and a limited amount of newly formed bone tissue. In the BG group, the bone defect region was mostly covered with fibrous tissue, while a greater extent of new bone formation was observed at the peripheral defects. Conversely, in the MTBG group, abundant new bone tissue formed throughout the entire defect site, exhibiting a bone structure and mineralization level comparable to those of the surrounding native bone tissue (Fig. 3D). The osteogenic capability was further confirmed by assessing the expression levels of RUNX2, OCN and collagen I. As illustrated in Fig. 3E and Fig. S10, the MTBG group exhibited a greater expression levels of RUNX2, OCN and collagen I compared with those in the BG or control group, suggesting robust and advanced bone formation.

3.3. MTBG alleviates BMSCs senescence

BMSCs senescence was induced according to a previous study [33]. The cells were then processed for transcriptome analysis by RNA sequencing. Kyoto Encyclopedia of Genes and Genomes (KEGG) enrichment analysis revealed significant increases in metabolic, cellular senescence, MAPK signaling, and p53 signaling pathways (Fig. S11), indicating cellular senescence.

The representative bright-field microscopy images depicted in Fig. 4A demonstrated that the aging cells lost their typical spindle morphological features and exhibited a flattened or irregular cell morphology with obvious pseudopodia. After treatment with melatonin or MTBG, the cells exhibited spindle-shaped characteristics similar to those of normal cells, whereas BG had no discernible impact on cell morphology. Additionally, melatonin or MTBG significantly reduced β-galactosidase staining and the protein expression of p16, p21 and p53 levels in aging BMSCs, confirming their efficacy in alleviating cellular senescence. Conversely, BG did not noticeably delay cellular senescence (Fig. 4B, E–H and J). Alizarin red staining demonstrated that both BG and melatonin enhanced calcium deposition in senescent BMSCs, with MTBG exhibiting the greatest effect (Fig. 4C and I). Evaluations of the gene and protein expression levels of OCN further confirmed the robust osteogenic potential of MTBG (Fig. 4D and Fig. S12).

3.4. MTBG enhances the mitochondrial function of senescent BMSCs

Based on the aforementioned results, in comparison to BG, MTBG exhibited superior potential in promoting aged bone formation due to its enhanced ability to delay cellular senescence. Therefore, we further investigated the mechanisms by which MTBG alleviates cellular senescence. Transcriptome sequencing was subsequently performed. A total of 155 downregulated genes and 130 upregulated genes were identified, as depicted in Fig. 5A. KEGG enrichment analysis revealed that the differently expressed genes (DEGs) were involved mainly in pathways associated with mitochondrial function, including calcium signaling, the mTOR signaling pathway, and metabolic pathways (Fig. 5B). The enrichment analysis suggested that MTBG may alleviate senescence by regulating mitochondrial homeostasis and metabolism. Therefore, a series of assays related to mitochondrial function were conducted. As shown in Fig. 5D, TEM images revealed the presence of mitochondria with swollen and vacuolated morphologies, exhibiting an irregular, dilated, and asymmetrical distribution of cristae in the aging cells. In contrast, following MTBG treatment, the mitochondria restored elongated tubular shapes and straight, parallel cristae that were comparable to those observed in the normal group. The intracellular and mitochondrial ROS levels were subsequently assessed. Immunofluorescence staining revealed significant accumulation levels of intracellular and mitochondrial ROS in the aging group, whereas treatment with MTBG effectively decreased the ROS levels (Fig. 5C and Fig. S13). Flow cytometry analysis further confirmed that the percentage of DCFH-DA-labeled cells in the MTBG group was significantly reduced (Fig. 5E and H). In addition, MTBG significantly enhanced ATP level in aging

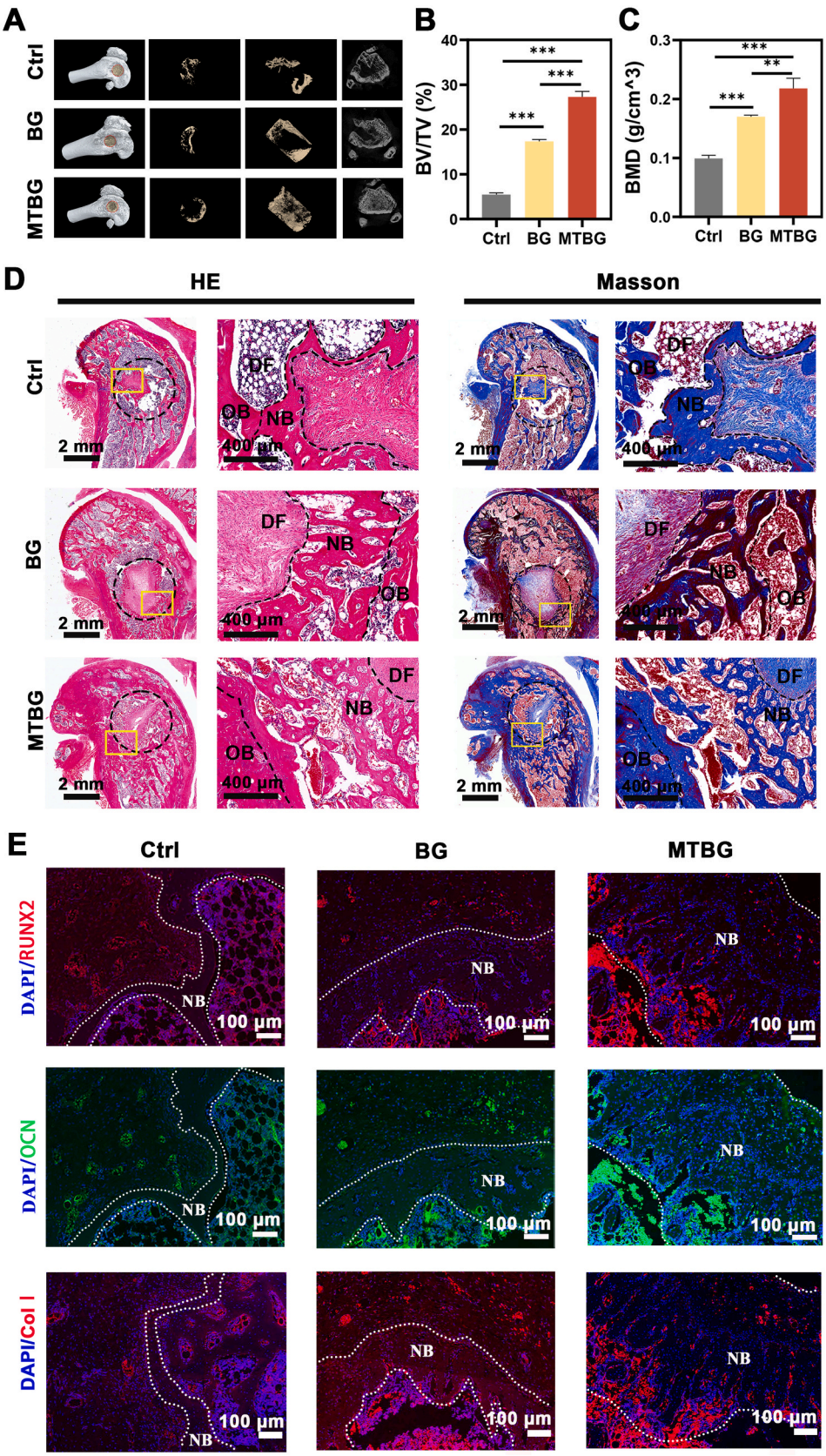

(caption on next page)

Fig. 3. *In vivo* evaluation of bone regeneration using femoral bone defects in an aged rat model. (A) Reconstructed micro-CT images of the femur defects including overall view, top view, side view and 2-dimensional cross-sectional sections; (B) Quantitative analysis of the regenerated bone tissues by measuring the bone volume to total volume (BV/TV); (C) Quantitative analysis of the regenerated bone tissues by measuring the bone mineral density (BMD); (D) Images of the defects with surrounding tissue stained with H&E and Masson's staining: the left column shows a general view of the profile; the right one presents the magnified view of the yellow box in the left column; (E) Immunofluorescence staining of osteogenesis-related markers after implantation for 6 weeks. Abbreviations are new bone (NB), old bone (OB) and defect (DF). $^{**}P < 0.01$, $^{***}P < 0.001$. (For interpretation of the references to colour in this figure legend, the reader is referred to the Web version of this article.)

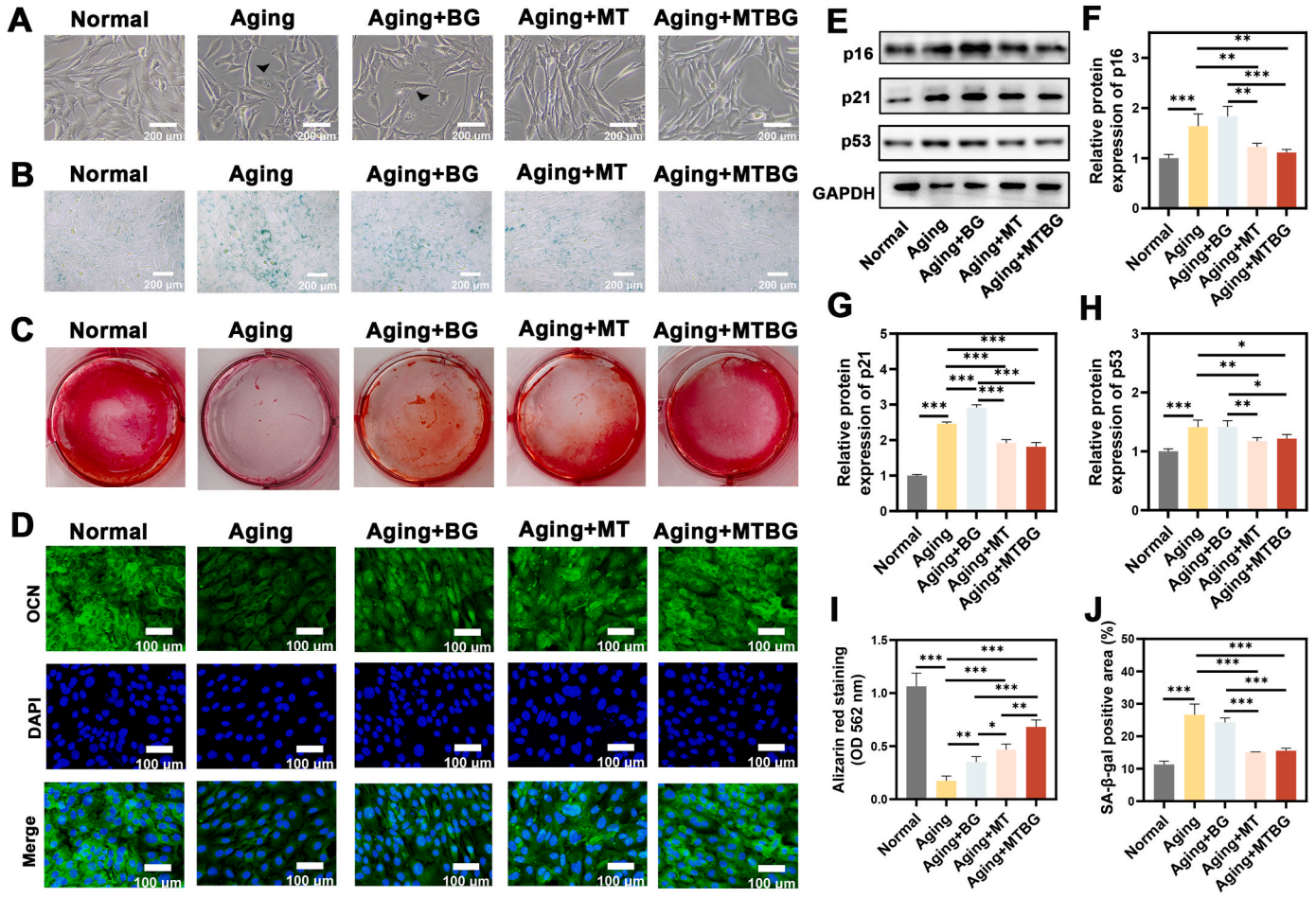

Fig. 4. MTBG alleviates BMSCs senescence and promotes osteogenic capacity. (A) Cell morphology observed by light microscopy. Black triangular arrows indicate the senescent cell; (B) β-galactosidase staining of BMSCs; (C) ARS staining of BMSCs; (D) Immunofluorescence staining images of OCN; (E) Protein expression levels of p16, p21 and p53; (F–H) Semiquantitative analysis of p16, p21 and p53; (I) Semiquantitative analysis of ARS staining; (J) Quantitative analysis of β-gal staining. $^{*}P < 0.05$, $^{**}P < 0.01$, $^{***}P < 0.001$.

BMSCs (Fig. 5J). JC-1 is a reliable indicator for detecting mitochondrial membrane potential in BMSCs. Distinct monomeric JC-1 was observed within the mitochondria of aging cells, whereas a greater abundance of JC-1 aggregates was detected within cellular mitochondria after MTBG treatment (Fig. 5F). The red/green fluorescence ratio of the mitochondrial membrane potential significantly increased after MTBG treatment, as confirmed by flow cytometry analysis (Fig. 5G and I). Taken together, these data indicate that MTBG effectively restores the mitochondrial function of senescent BMSCs.

3.5. MTBG facilitates mitochondrial transfer by TNTs

The term "mitochondrial transfer" refers to the transportation of mitochondria between cells [28] (Fig. 6A). The transfer of mitochondria through TNTs has been associated with the restoration of dysfunctional mitochondria [34]. As shown in Fig. 6C, a typical actin–TNT-labeled structure (red arrow) was observed intercellularly, with longer TNT length noted in aging and MTBG treated aging cells. Confocal z-stack images revealed mitochondria located within the TNTs, as indicated by the red fluorescence-labeled mitochondria observed in the green fluorescence-labeled TNT structures (Fig. 6D). To further elucidate the phenomenon of intercellular mitochondrial transfer, cells labeled with MitoTracker Red were cocultured with cells labeled with CFDA SE at a 1:1 ratio (Fig. 6B). MitoTracker Red-labeled mitochondria were observed in CFDA SE-labeled cells, providing evidence of intercellular mitochondrial transfer, as depicted in Fig. 6E. Miro1, the key regulator of mitochondrial transfer, was significantly upregulated in the MTBG group, indicating enhanced mitochondrial transfer. PGC1α expression was also increased after MTBG treatment (Fig. 6F–H and Fig. S14). The *in vivo* results further demonstrated significantly greater numbers of Miro1 (red)- and PGC1α (green)-positive cells (triangular arrow) at the site of newly formed bone in the MTBG group than in the BG and blank groups, indicating an increase in mitochondrial transfer and biogenesis (Fig. 6I and J).

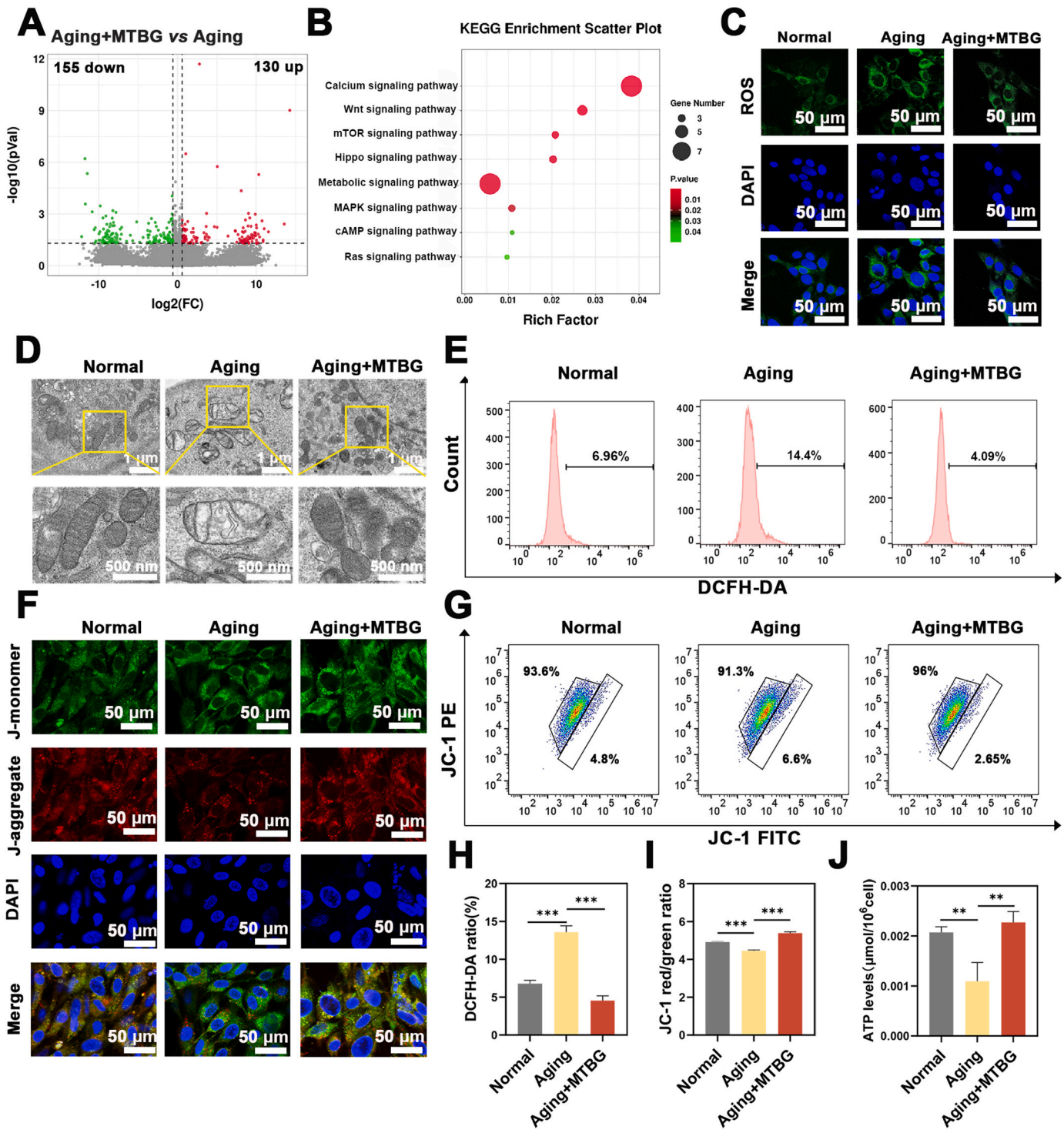

Fig. 5. MTBG enhances the mitochondrial function of senescent BMSCs. (A) Volcano plot of the differentially expressed genes between Aging + MTBG and Aging groups (≥2-fold difference, *P* value < 0.05); (B) The gene enrichment KEGG pathways analysis of Aging + MTBG *vs* Aging; (C) Immunofluorescence staining images of intracellular ROS by DCFH-DA probe; (D) Representative TEM images showing the nanostructures of mitochondria; (E) Flow cytometry histograms showing the intracellular ROS levels; (F) Immunofluorescence staining images of mitochondrial membrane potential detected by JC-1 probe; (G) Flow cytometry histograms showing the mitochondrial membrane potential; (H) Quantitative analysis of flow cytometry assays showing the intracellular ROS level; (I) Quantitative analysis of flow cytometry assays showing mitochondrial membrane potential; (J) Intracellular ATP levels of BMSCs determined by ATP assays. $^{**}P < 0.01$, $^{***}P < 0.001$.

The TNT inhibitor cytochalasin B (CB) was used to further elucidate the involvement of TNTs in facilitating mitochondrial transfer (Fig. 7A). As depicted in Fig. 7B, CB significantly attenuated the facilitating effect of MTBG on mitochondrial transfer. Moreover, CB compromised the protective effect of MTBG on mitochondria, as evidenced by elevated ROS levels (Fig. 7D, F–G), decreased mitochondrial membrane potential (Fig. 7C and H), and reduced ATP production (Fig. 7E). These findings substantiate the participation of TNTs in facilitating mitochondrial transfer and mediating mitochondrial protection in senescent BMSCs.

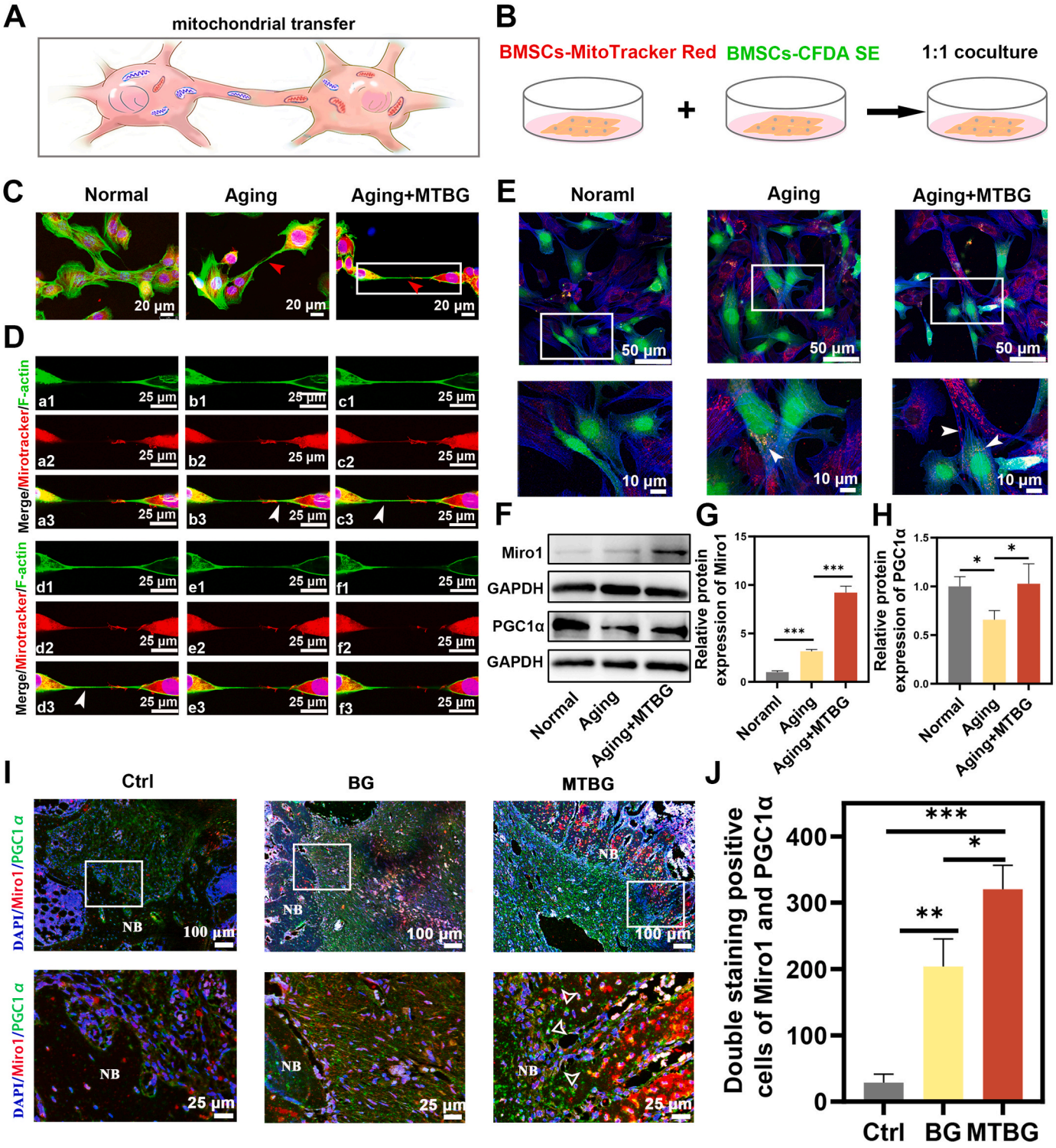

Fig. 6. MTBG induces TNTs formation and mitochondria transfer in senescent BMSCs. (A) Schematic illustration of mitochondrial transfer; (B) Schematic representation of the coculture experimental design for the detection of mitochondrial transfer; (C) Confocal images of co-staining with phalloidin (green) and MitoTracker Red (red). Red arrows indicate tunneling nanotubes (TNTs); (D) Z-stack images (a–f) of the white box area in Fig. 6C show mitochondria (white arrows) inside TNT structures; (E) Immunofluorescence staining of mitochondrial transfer from cells labeled with MitoTracker Red to cells labeled with CFDA SE. The lower row presents the magnified view of the white box in the upper row. White arrows indicate the transferred mitochondria; (F) Protein expression of Miro1 and PGC1α; (G) Semiquantitative analysis of Miro1; (H) Semiquantitative analysis of PGC1α; (I) Double-stained immunofluorescence images of Miro1 and PGC1α of the femur samples. The lower row presents the magnified view of the white box in the upper row; White triangular arrows indicate the co-localizing cells. Abbreviation is new bone (NB); (J) Quantification of the Miro1/PGC1α double-positive cell number. $^{*}P < 0.05$, $^{**}P < 0.01$, $^{***}P < 0.001$. (For interpretation of the references to colour in this figure legend, the reader is referred to the Web version of this article.)

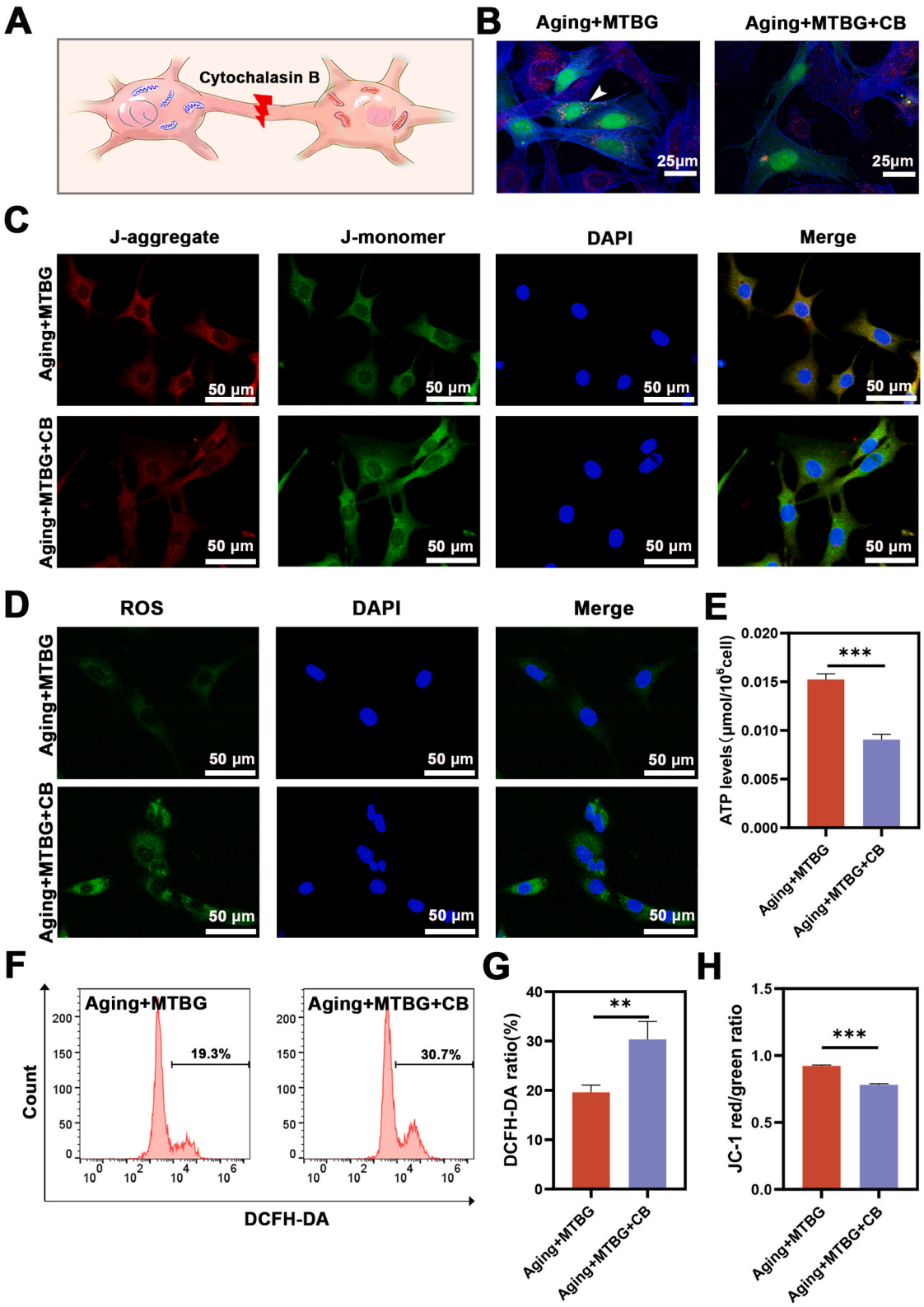

Fig. 7. Cytochalasin B mitigates the effect of MTBG on enhancing mitochondrial transfer and mitochondrial protection in senescent BMSCs. (A) Schematic illustration of cytochalasin B blocking the transfer of mitochondria; (B) Immunofluorescence staining of the transferred mitochondria from cells labeled with MitoTracker Red to cells labeled with CFDA SE. White arrow indicates the transferred mitochondria; (C) Immunofluorescence staining images of mitochondrial membrane potential detected by JC-1 probe; (D) Immunofluorescence staining images of intracellular ROS by DCFH-DA probe; (E) Intracellular ATP levels of BMSCs determined by ATP assays; (F) Flow cytometry histograms showing the intracellular ROS levels using DCFH-DA probe; (G) Quantitative analysis of flow cytometry assays showing the percentage of DCFH-DA-labeled cells; (H) Quantitative analysis of flow cytometry assays showing mitochondrial membrane potential. $^{**}P < 0.01$, $^{***}P < 0.001$. (For interpretation of the references to colour in this figure legend, the reader is referred to the Web version of this article.)

4. Discussion

Bone defect repair in the elderly population is a global challenge. In this study, we successfully synthesized MTBG, which rejuvenated senescent BMSCs, leading to the significant acceleration of bone defect repair in aged rats. Additionally, we elucidated a new mechanism by which MTBG promotes the formation of TNTs and facilitates mitochondrial transfer in senescent BMSCs, thereby restoring mitochondrial function.

The exceptional specific surface area and pore volume of mesoporous BG render it an optimal candidate for loading bioactive molecules and drugs [35]. The prevailing belief is that a surface area of 200–350 $m^2 g^{-1}$, along with a mesopore size ranging from 3 to 5 nm, would create an optimal environment for adsorbing various biomolecules and drugs [32]. In this study, the MTBG synthesized had a mesoporous structure with a mesopore size approximately of 4 nm. Additionally, the MTBG was effectively loaded with melatonin and exhibited sustained release kinetics. Furthermore, the osteogenic capacity of the MTBG microspheres was superior to that of the BG microspheres in aged rats. Melatonin released from the MTBG microspheres evidently plays a significant role in accelerating bone regeneration.

To further investigate the mechanisms by which MTBG promotes osteogenesis, a series of *in vitro* experiments were conducted to compare the effects of BG, melatonin, and MTBG on cellular senescence and osteogenic capacity. Senescent cells display an enlarged and flattened morphology, accompanied by a limited proliferative capacity [36]. MTBG and melatonin restored the morphology of senescent BMSCs. The cyclin-dependent kinase inhibitors p16, p21 and p53 are widely acknowledged as biomarkers of aging and cellular senescence [37,38], and β-galactosidase activity increases with age [39]. The protein levels of p16, p21 and p53 in senescent BMSCs were significantly reduced by MTBG and melatonin, and the intensity of β-galactosidase staining decreased, indicating the effective alleviation of the aging process in BMSCs. However, BG did not exert any discernible impact on the delay of cellular senescence. In addition, both BG and melatonin promoted osteogenic differentiation in aging cells, while MTBG exhibited the greatest effect. Combined with the *in vivo* results, these findings suggest that MTBG releases not only Ca, Si, and P ions to enhance calcium deposition but also melatonin to alleviate cellular senescence, thereby further promoting osteogenesis.

Among the various factors contributing to senescence, mitochondrial dysfunction has emerged as a prominent contributor to the aging process [40]. Significant alterations in mitochondrial morphology, perturbed dynamics, heightened ROS production, and compromised functioning of the electron transport chain (ETC) and ATP synthesis are intricately linked to mitochondrial dysfunction, thereby leading to cellular senescence [21,41]. Therefore, maintaining optimal mitochondrial function is crucial for preventing cellular senescence. Mitochondrial cristae increase the surface area of the inner membrane, facilitating higher abundances of proteins associated with mitochondrial respiration [42]. Consequently, remodeling of the structure of the mitochondrial cristae structure is closely linked to mitochondrial function [43]. In the present study, MTBG restored the irregular, dilated and discontinuous cristae in senescent cells to a continuous configuration. A decrease in the mitochondrial membrane potential has been observed during aging, indicating that mitochondria are impaired in senescent cells [44]. In addition to scavenging ROS, MTBG also enhanced the mitochondrial membrane potential and the ATP production of senescent BMSCs, providing compelling evidence for the restoration of mitochondrial function by MTBG in these cells.

A novel and intriguing finding of this study is that MTBG promotes intercellular mitochondrial transfer between senescent BMSCs. Studies have shown that intercellular mitochondrial transfer occurs in numerous tissues, resulting in a significant increase in ATP production in the recipient cells [30]. This finding suggested the functional incorporation of exogenous mitochondria into the pool of endogenous mitochondria within the recipient cells [45]. Mitochondrial transfer has emerged as a promising therapeutic strategy owing to its ability to restore the bioenergetic needs of injured cells [46,47]. Mesenchymal stem cells (MSCs) preferentially release their functional mitochondria toward damaged cells, which subsequently fuse with the mitochondrial network and facilitate the recovery of mitochondrial quality in these injured cells [48,49]. In addition to functional mitochondria, damaged mitochondria can also be delivered to neighboring cells for degradation, recycling, or even signaling rescue [50,51]. For instance, damaged neurons transfer damaged mitochondria to astrocytes for degradation, thereby preserving optimal mitochondrial function and preventing cellular stress [52]. Melatonin was found to promote mitochondrial transfer between injured HT22 cells and restructure their mitochondrial network, ultimately resulting in cellular recovery [53]. We speculated that the incorporation of melatonin into MTBG may contribute to the facilitation of mitochondrial transfer among aging cells. However, it remains unclear how these transferred mitochondria contribute to the restoration of the mitochondrial network. Further investigations are needed to elucidate the regulatory mechanism governing the fate of transferred mitochondria in cells.

Among the various structures that mediate intercellular mitochondrial transfer, TNTs are currently considered the major cellular structure [31]. They are dynamic membranous protrusions containing actin and are characterized by a diameter of 20–500 nm and lengths of up to 100 μm [54,55]. The formation of TNTs is a main feature of cells under stress conditions, such as senescence, ROS accumulation and inflammation [30,53]. Confocal laser microscopy enables precise monitoring of TNT formation. Live imaging of TNT-connected cells can be valuable for tracking the dynamic transfer of mitochondria. Another quantitative method to investigate intercellular mitochondria transfer is flow cytometry, which provides a more direct and faster quantitative analysis but is inferior compared to microscopy analysis [56]. In this study, TNTs formation increased in aging cells, which is consistent with previous findings. Z-stack laser confocal microscopy was employed to confirm the presence of mitochondria within the TNTs. Furthermore, treatment with cytochalasin B, a TNT inhibitor, significantly attenuated MTBG-mediated increase in mitochondrial transfer and the restoration of mitochondrial function, providing further evidence that intercellular mitochondrial transfer occurs via TNTs.

Although the precise regulatory mechanism of mitochondrial transfer remains elusive, mitochondrial Rho-GTPase 1 (Miro1), an outer mitochondrial membrane protein, is considered a key player in mitochondrial transfer via TNTs [57]. Miro1 interacts with the kinesin motor protein KLF5, as well as TRAK1 and TRAK2, to form a motor adaptor complex that facilitates mitochondrial transport machinery and regulates mitochondrial movement on microtubules [58]. Overexpression of Miro1 in MSCs resulted in enhanced TNTs formation and increased mitochondrial transfer to cocultured astrocytes *in vitro*, leading to improved mitochondrial biogenesis [59]. PGC1α is the master regulator of mitochondrial biogenesis [60]. The protein levels of both Miro1 and PGC1α were significantly upregulated following MTBG treatment. Additionally, the MTBG group demonstrated the highest coexpression of Miro1 and PGC1α in the bone defect samples, providing compelling evidence linking mitochondrial transfer to an increase in mitochondrial biogenesis *in vivo*.

5. Conclusion

In this study, a sustained release system of melatonin and bioactive ions was successfully prepared. MTBG significantly accelerated aged bone regeneration by improving mitochondrial function and thus rejuvenating senescent BMSCs. More specifically, a novel mechanism in which MTBG induces the formation of TNTs and facilitates mitochondrial transfer among senescent BMSCs, ultimately enhancing mitochondrial biogenesis was elucidated. In summary, MTBG provides new avenues for material design in the fields of tissue engineering and

regenerative medicine for elderly individuals.

Ethics approval and consent to participate

The study was approved by the ethics committee (Full name: GuangDong Pharmaceutical University Experimental Animal Ethics Committee Inspection) (Reference number: gdpulacspf2022112), GuangDong Pharmaceutical University, China.

CRediT authorship contribution statement

Huacui Xiong: Writing – review & editing, Writing – original draft, Methodology, Data curation. **Huanhuan Qiu:** Writing – review & editing, Methodology, Data curation. **Chunhui Wang:** Methodology, Data curation. **Yonghao Qiu:** Methodology, Data curation. **Shuyi Tan:** Writing – review & editing, Data curation. **Ke Chen:** Project administration. **Fujian Zhao:** Writing – review & editing, Project administration, Funding acquisition. **Jinlin Song:** Supervision, Project administration, Funding acquisition.

Declaration of competing interest

The authors declare that they have no known competing financial interests or personal relationships that could have appeared to influence the work reported in this paper.

Data availability

Data will be made available on request.

Acknowledgements

This work was supported by the National Natural Science Foundation of China (No. 32171311, 32000933), the Young Talent Support Project of Guangzhou Association for Science and Technology (No. QT-2023-020) and the Chongqing Young and Middle-Aged Medical Excellence Team ([2022] No. 15).

Appendix A. Supplementary data

Supplementary data to this article can be found online at https://doi.org/10.1016/j.mtbio.2024.101175.

References

[1] A.C. van der Burgh, C.E. de Keyser, M.C. Zillikens, B.H. Stricker, The effects of osteoporotic and non-osteoporotic medications on fracture risk and bone mineral density, Drugs 81 (2021) 1831–1858, https://doi.org/10.1007/s40265-021-01625-8.

[2] J.N. Farr, S. Khosla, Cellular senescence in bone, Bone 121 (2019) 121–133, https://doi.org/10.1016/j.bone.2019.01.015.

[3] J. Cui, Y. Shibata, T. Zhu, J. Zhou, J. Zhang, Osteocytes in bone aging: advances, challenges, and future perspectives, Ageing Res. Rev. 77 (2022) 101608, https://doi.org/10.1016/j.arr.2022.101608.

[4] A. Pinna, M. Torki Baghbaderani, V. Vigil Hernandez, P. Naruphontjirakul, S. Li, T. McFarlane, D. Hachim, M.M. Stevens, A.E. Porter, J.R. Jones, Nanoceria provides antioxidant and osteogenic properties to mesoporous silica nanoparticles for osteoporosis treatment, Acta Biomater. 122 (2021) 365–376, https://doi.org/10.1016/j.actbio.2020.12.029.

[5] N.K. Zarrin, F. Mottaghitalab, R.L. Reis, S.C. Kundu, M. Farokhi, Thermosensitive chitosan/poly(N-isopropyl acrylamide) nanoparticles embedded in aniline pentamer/silk fibroin/polyacrylamide as an electroactive injectable hydrogel for healing critical-sized calvarial bone defect in aging rat model, Int. J. Biol. Macromol. 213 (2022) 352–368, https://doi.org/10.1016/j.ijbiomac.2022.05.176.

[6] F. Zhao, W. Xie, W. Zhang, X. Fu, W. Gao, B. Lei, X. Chen, 3D printing nanoscale bioactive glass scaffolds enhance osteoblast migration and extramembranous osteogenesis through stimulating immunomodulation, Adv. Healthcare Mater. 7 (2018) e1800361, https://doi.org/10.1002/adhm.201800361.

[7] S. Liu, Z. Han, J.N. Hao, D. Zhang, X. Li, Y. Cao, J. Huang, Y. Li, Engineering of a NIR-activable hydrogel-coated mesoporous bioactive glass scaffold with dual-mode parathyroid hormone derivative release property for angiogenesis and bone regeneration, Bioact. Mater. 26 (2023) 1–13, https://doi.org/10.1016/j.bioactmat.2023.02.008.

[8] V. Lalzawmliana, A. Anand, M. Roy, B. Kundu, S.K. Nandi, Mesoporous bioactive glasses for bone healing and biomolecules delivery, Mater. Sci. Eng., C 106 (2020) 110180, https://doi.org/10.1016/j.msec.2019.110180.

[9] S. Gupta, S. Majumdar, S. Krishnamurthy, Bioactive glass: a multifunctional delivery system, J. Contr. Release 335 (2021) 481–497, https://doi.org/10.1016/j.jconrel.2021.05.043.

[10] Y. Byeon, H.J. Lee, H.Y. Lee, K. Back, Cloning and functional characterization of the Arabidopsis N-acetylserotonin O-methyltransferase responsible for melatonin synthesis, J. Pineal Res. 60 (2016) 65–73, https://doi.org/10.1111/jpi.12289.

[11] A. Galano, R.J. Reiter, Melatonin and its metabolites vs oxidative stress: from individual actions to collective protection, J. Pineal Res. 65 (2018) e12514, https://doi.org/10.1111/jpi.12514.

[12] C. Fan, J. Feng, C. Tang, Z. Zhang, Y. Feng, W. Duan, M. Zhai, Z. Yan, L. Zhu, L. Feng, H. Zhu, E. Luo, Melatonin suppresses ER stress-dependent proapoptotic effects via AMPK in bone mesenchymal stem cells during mitochondrial oxidative damage, Stem Cell Res. Ther. 11 (2020) 442, https://doi.org/10.1186/s13287-020-01948-5.

[13] Z. Zhang, S. Tang, Y. Jiang, F. Long, F. He, J. Liu, S. Gu, Y. Lu, Z. Yin, Oxidative stress induces meiotic defects of oocytes in a mouse psoriasis model, Cell Death Dis. 13 (2022) 474, https://doi.org/10.1038/s41419-022-04948-w.

[14] Y. Xie, N. Han, F. Li, L. Wang, G. Liu, M. Hu, S. Wang, X. Wei, J. Guo, H. Jiang, J. Wang, X. Li, Y. Wang, J. Wang, X. Bian, Z. Zhu, H. Zhang, C. Liu, X. Liu, Z. Liu, Melatonin enhances osteoblastogenesis of senescent bone marrow stromal cells through NSD2-mediated chromatin remodelling, Clin. Transl. Med. 12 (2022) e746, https://doi.org/10.1002/ctm2.746.

[15] B. Wang, H. Wen, W. Smith, D. Hao, B. He, L. Kong, Regulation effects of melatonin on bone marrow mesenchymal stem cell differentiation, J. Cell. Physiol. 234 (2019) 1008–1015, https://doi.org/10.1002/jcp.27090.

[16] Z.M. Chu, H.B. Li, S.X. Sun, Y.C. Jiang, B. Wang, Y.F. Dong, Melatonin promotes osteoblast differentiation of bone marrow mesenchymal stem cells in aged rats, Eur. Rev. Med. Pharmacol. Sci. 21 (2017) 4446–4456.

[17] J.A. Schafer, S. Bozkurt, J.B. Michaelis, K. Klann, C. Munch, Global mitochondrial protein import proteomics reveal distinct regulation by translation and translocation machinery, Mol. Cell 82 (2022) 435–446 e437, https://doi.org/10.1016/j.molcel.2021.11.004.

[18] L. Fernandez-Mosquera, K.F. Yambire, R. Couto, L. Pereyra, K. Pabis, A. H. Ponsford, C.V. Diogo, M. Stagi, I. Milosevic, N. Raimundo, Mitochondrial respiratory chain deficiency inhibits lysosomal hydrolysis, Autophagy 15 (2019) 1572–1591, https://doi.org/10.1080/15548627.2019.1586256.

[19] L.P. Diebold, H.J. Gil, P. Gao, C.A. Martinez, S.E. Weinberg, N.S. Chandel, Mitochondrial complex III is necessary for endothelial cell proliferation during angiogenesis, Nat. Metab. 1 (2019) 158–171, https://doi.org/10.1038/s42255-018-0011-x.

[20] J. Lv, Y. Yi, Y. Qi, C. Yan, W. Jin, L. Meng, D. Zhang, W. Jiang, Mitochondrial homeostasis regulates definitive endoderm differentiation of human pluripotent stem cells, Cell Death Dis. 8 (2022) 69, https://doi.org/10.1038/s41420-022-00867-z.

[21] S.K. Ghosh-Choudhary, J. Liu, T. Finkel, The role of mitochondria in cellular senescence, Faseb. J. 35 (2021) e21991, https://doi.org/10.1096/fj.202101462R.

[22] L. Habiballa, H. Salmonowicz, J.F. Passos, Mitochondria and cellular senescence: implications for musculoskeletal ageing, Free Radic. Biol. Med. 132 (2019) 3–10, https://doi.org/10.1016/j.freeradbiomed.2018.10.417.

[23] M. Calvo-Rodriguez, B.J. Bacskai, Mitochondria and calcium in alzheimer's disease: from cell signaling to neuronal cell death, Trends Neurosci. 44 (2021) 136–151, https://doi.org/10.1016/j.tins.2020.10.004.

[24] M. Manevski, T. Muthumalage, D. Devadoss, I.K. Sundar, Q. Wang, K.P. Singh, H. J. Unwalla, H.S. Chand, I. Rahman, Cellular stress responses and dysfunctional Mitochondrial-cellular senescence, and therapeutics in chronic respiratory diseases, Redox Biol. 33 (2020) 101443, https://doi.org/10.1016/j.redox.2020.101443.

[25] V.I. Korolchuk, S. Miwa, B. Carroll, T. von Zglinicki, Mitochondria in cell senescence: is mitophagy the weakest link? EBioMedicine 21 (2017) 7–13, https://doi.org/10.1016/j.ebiom.2017.03.020.

[26] J. Chapman, E. Fielder, J.F. Passos, Mitochondrial dysfunction and cell senescence: deciphering a complex relationship, FEBS Lett. 593 (2019) 1566–1579, https://doi.org/10.1002/1873-3468.13498.

[27] R. Di Micco, V. Krizhanovsky, D. Baker, F. d'Adda di Fagagna, Cellular senescence in ageing: from mechanisms to therapeutic opportunities, Nat. Rev. Mol. Cell Biol. 22 (2021) 75–95, https://doi.org/10.1038/s41580-020-00314-w.

[28] D. Liu, Y. Gao, J. Liu, Y. Huang, J. Yin, Y. Feng, L. Shi, B.P. Meloni, C. Zhang, M. Zheng, J. Gao, Intercellular mitochondrial transfer as a means of tissue revitalization, Signal Transduct. Targeted Ther. 6 (2021) 65, https://doi.org/10.1038/s41392-020-00440-z.

[29] S. Shanmughapriya, D. Langford, K. Natarajaseenivasan, Inter and Intracellular mitochondrial trafficking in health and disease, Ageing Res. Rev. 62 (2020) 101128, https://doi.org/10.1016/j.arr.2020.101128.

[30] Y. Liu, T. Fu, G. Li, B. Li, G. Luo, N. Li, Q. Geng, Mitochondrial transfer between cell crosstalk - an emerging role in mitochondrial quality control, Ageing Res. Rev. 91 (2023) 102038, https://doi.org/10.1016/j.arr.2023.102038.

[31] A. Sartori-Rupp, D. Cordero Cervantes, A. Pepe, K. Gousset, E. Delage, S. Corroyer-Dulmont, C. Schmitt, J. Krijnse-Locker, C. Zurzolo, Correlative cryo-electron microscopy reveals the structure of TNTs in neuronal cells, Nat. Commun. 10 (2019) 342, https://doi.org/10.1038/s41467-018-08178-7.

[32] L. Liu, F. Zhao, X. Chen, M. Luo, Z. Yang, X. Cao, G. Miao, D. Chen, X. Chen, Local delivery of FTY720 in mesoporous bioactive glass improves bone regeneration by synergistically immunomodulating osteogenesis and osteoclastogenesis, J. Mater. Chem. B 8 (2020) 6148–6158, https://doi.org/10.1039/d0tb00982b.
[33] S. Wedel, I. Martic, N. Hrapovic, S. Fabre, C.T. Madreiter-Sokolowski, T. Haller, G. Pierer, C. Ploner, P. Jansen-Durr, M. Cavinato, tBHP treatment as a model for cellular senescence and pollution-induced skin aging, Mech. Ageing Dev. 190 (2020) 111318, https://doi.org/10.1016/j.mad.2020.111318.
[34] M.L. Vignais, A. Caicedo, J.M. Brondello, C. Jorgensen, Cell connections by tunneling nanotubes: effects of mitochondrial trafficking on target cell metabolism, homeostasis, and response to therapy, Stem Cell. Int. 2017 (2017) 6917941, https://doi.org/10.1155/2017/6917941.
[35] A. El-Fiqi, N. Mandakhbayar, S.B. Jo, J.C. Knowles, J.H. Lee, H.W. Kim, Nanotherapeutics for regeneration of degenerated tissue infected by bacteria through the multiple delivery of bioactive ions and growth factor with antibacterial/angiogenic and osteogenic/odontogenic capacity, Bioact. Mater. 6 (2021) 123–136, https://doi.org/10.1016/j.bioactmat.2020.07.010.
[36] M. Montes, M. Lubas, F.S. Arendrup, B. Mentz, N. Rohatgi, S. Tumas, L.M. Harder, A.J. Skanderup, J.S. Andersen, A.H. Lund, The long non-coding RNA MIR31HG regulates the senescence associated secretory phenotype, Nat. Commun. 12 (2021) 2459, https://doi.org/10.1038/s41467-021-22746-4.
[37] H. Safwan-Zaiter, N. Wagner, J.F. Michiels, K.D. Wagner, Dynamic spatiotemporal expression pattern of the senescence-associated factor p16Ink4a in development and aging, Cells 11 (2022), https://doi.org/10.3390/cells11030541.
[38] S.C. Yang, H.Y. Chen, W.L. Chuang, H.C. Wang, C.P. Hsieh, Y.F. Huang, Different cell responses to hinokitiol treatment result in senescence or apoptosis in human osteosarcoma cell lines, Int. J. Mol. Sci. 23 (2022), https://doi.org/10.3390/ijms23031632.
[39] F. Debacq-Chainiaux, J.D. Erusalimsky, J. Campisi, O. Toussaint, Protocols to detect senescence-associated beta-galactosidase (SA-betagal) activity, a biomarker of senescent cells in culture and in vivo, Nat. Protoc. 4 (2009) 1798–1806, https://doi.org/10.1038/nprot.2009.191.
[40] S. Srivastava, The mitochondrial basis of aging and age-related disorders, Genes 8 (2017), https://doi.org/10.3390/genes8120398.
[41] H. Martini, J.F. Passos, Cellular senescence: all roads lead to mitochondria, FEBS J. 290 (2023) 1186–1202, https://doi.org/10.1111/febs.16361.
[42] S. Cogliati, J.A. Enriquez, L. Scorrano, Mitochondrial cristae: where beauty meets functionality, Trends Biochem. Sci. 41 (2016) 261–273, https://doi.org/10.1016/j.tibs.2016.01.001.
[43] C. Hu, L. Shu, X. Huang, J. Yu, L. Li, L. Gong, M. Yang, Z. Wu, Z. Gao, Y. Zhao, L. Chen, Z. Song, OPA1 and MICOS Regulate mitochondrial crista dynamics and formation, Cell Death Dis. 11 (2020) 940, https://doi.org/10.1038/s41419-020-03152-y.
[44] T.T. Lee, P.L. Chen, M.P. Su, J.C. Li, Y.W. Chang, R.W. Liu, H.F. Juan, J.M. Yang, S. P. Chan, Y.C. Tsai, S. von Stockum, E. Ziviani, A. Kamikouchi, H.D. Wang, C. H. Chen, Loss of Fis1 impairs proteostasis during skeletal muscle aging in Drosophila, Aging Cell 20 (2021) e13379, https://doi.org/10.1111/acel.13379.
[45] R.Z. Lin, G.B. Im, A.C. Luo, Y. Zhu, X. Hong, J. Neumeyer, H.W. Tang, N. Perrimon, J.M. Melero-Martin, Mitochondrial transfer mediates endothelial cell engraftment through mitophagy, Nature 629 (2024) 660–668, https://doi.org/10.1038/s41586-024-07340-0.
[46] S. Paliwal, R. Chaudhuri, A. Agrawal, S. Mohanty, Regenerative abilities of mesenchymal stem cells through mitochondrial transfer, J. Biomed. Sci. 25 (2018) 31, https://doi.org/10.1186/s12929-018-0429-1.
[47] D. Jiang, F.X. Chen, H. Zhou, Y.Y. Lu, H. Tan, S.J. Yu, J. Yuan, H. Liu, W. Meng, Z. B. Jin, Bioenergetic crosstalk between mesenchymal stem cells and various ocular cells through the intercellular trafficking of mitochondria, Theranostics 10 (2020) 7260–7272, https://doi.org/10.7150/thno.46332.
[48] S. Jin, N. Cordes, ATM controls DNA repair and mitochondria transfer between neighboring cells, Cell Commun. Signal. 17 (2019) 144, https://doi.org/10.1186/s12964-019-0472-x.
[49] C.G. Gabelein, Q. Feng, E. Sarajlic, T. Zambelli, O. Guillaume-Gentil, B. Kornmann, J.A. Vorholt, Mitochondria transplantation between living cells, PLoS Biol. 20 (2022) e3001576, https://doi.org/10.1371/journal.pbio.3001576.
[50] K. Hayakawa, E. Esposito, X. Wang, Y. Terasaki, Y. Liu, C. Xing, X. Ji, E.H. Lo, Transfer of mitochondria from astrocytes to neurons after stroke, Nature 535 (2016) 551–555, https://doi.org/10.1038/nature18928.
[51] M. Mahrouf-Yorgov, L. Augeul, C.C. Da Silva, M. Jourdan, M. Rigolet, S. Manin, R. Ferrera, M. Ovize, A. Henry, A. Guguin, J.P. Meningaud, J.L. Dubois-Rande, R. Motterlini, R. Foresti, A.M. Rodriguez, Mesenchymal stem cells sense mitochondria released from damaged cells as danger signals to activate their rescue properties, Cell Death Differ. 24 (2017) 1224–1238, https://doi.org/10.1038/cdd.2017.51.
[52] R. Lampinen, I. Belaya, L. Saveleva, J.R. Liddell, D. Rait, M.T. Huuskonen, R. Giniatullina, A. Sorvari, L. Soppela, N. Mikhailov, I. Boccuni, R. Giniatullin, M. Cruz-Haces, J. Konovalova, M. Koskuvi, A. Domanskyi, R.H. Hamalainen, G. Goldsteins, J. Koistinaho, T. Malm, S. Chew, K. Rilla, A.R. White, N. Marsh-Armstrong, K.M. Kanninen, Neuron-astrocyte transmitophagy is altered in Alzheimer's disease, Neurobiol. Dis. 170 (2022) 105753, https://doi.org/10.1016/j.nbd.2022.105753.
[53] M.G. Nasoni, S. Carloni, B. Canonico, S. Burattini, E. Cesarini, S. Papa, M. Pagliarini, P. Ambrogini, W. Balduini, F. Luchetti, Melatonin reshapes the mitochondrial network and promotes intercellular mitochondrial transfer via tunneling nanotubes after ischemic-like injury in hippocampal HT22 cells, J. Pineal Res. 71 (2021) e12747, https://doi.org/10.1111/jpi.12747.
[54] A. Rustom, R. Saffrich, I. Markovic, P. Walther, H.H. Gerdes, Nanotubular highways for intercellular organelle transport, Science 303 (2004) 1007–1010, https://doi.org/10.1126/science.1093133.
[55] M.W. Austefjord, H.H. Gerdes, X. Wang, Tunneling nanotubes: diversity in morphology and structure, Commun. Integr. Biol. 7 (2014) e27934, https://doi.org/10.4161/cib.27934.
[56] I. Saenz-de-Santa-Maria, J.M. Henderson, A. Pepe, C. Zurzolo, Identification and characterization of tunneling nanotubes for intercellular trafficking, Curr Protoc 3 (2023) e939, https://doi.org/10.1002/cpz1.939.
[57] G. Lopez-Domenech, C. Covill-Cooke, D. Ivankovic, E.F. Halff, D.F. Sheehan, R. Norkett, N. Birsa, J.T. Kittler, Miro proteins coordinate microtubule- and actin-dependent mitochondrial transport and distribution, EMBO J. 37 (2018) 321–336, https://doi.org/10.15252/embj.201696380.
[58] E.L. Eberhardt, A.V. Ludlam, Z. Tan, M.A. Cianfrocco, Miro: a molecular switch at the center of mitochondrial regulation, Protein Sci. 29 (2020) 1269–1284, https://doi.org/10.1002/pro.3839.
[59] V.A. Babenko, D.N. Silachev, V.A. Popkov, L.D. Zorova, I.B. Pevzner, E. Y. Plotnikov, G.T. Sukhikh, D.B. Zorov, Miro1 enhances mitochondria transfer from multipotent mesenchymal stem cells (MMSC) to neural cells and improves the efficacy of cell recovery, Molecules 23 (2018), https://doi.org/10.3390/molecules23030687.
[60] K. Kaarniranta, J. Kajdanek, J. Morawiec, E. Pawlowska, J. Blasiak, PGC-1alpha protects RPE cells of the aging retina against oxidative stress-induced degeneration through the regulation of senescence and mitochondrial quality control. The significance for AMD pathogenesis, Int. J. Mol. Sci. 19 (2018), https://doi.org/10.3390/ijms19082317.